

DOI:10.16356/j.1005-2615.2024.02.017

## 基于渐近均匀化的梯度板等效刚度数值计算

张德纲<sup>1</sup>, 顾铖璋<sup>2</sup>, 韦 啸<sup>2</sup>, 齐鹏飞<sup>2</sup>, 徐 亮<sup>1</sup>

(1. 南京航空航天大学航空学院, 南京 210016; 2. 上海宇航系统工程研究所结构系统研究室, 上海 201109)

**摘要:** 基于梯度板结构的渐近均匀化方法, 简化梯度板微单胞的单胞方程及等效刚度列式, 并推导其有限元求解列式, 实现梯度加筋板微结构等效刚度的高效数值求解。相比仅能处理矩形单胞的经典数值均匀化方法, 该方法可以处理一般平行四边形微结构, 具有更好的普适性。数值算例通过比对梯度加筋板及其对应的等效均质板挠度, 最大挠度数值相对误差均在 5% 以内, 验证了所提数值方法的正确性及可行性。

**关键词:** 渐近均匀化; 梯度加筋板; 映射函数; 等效刚度; 数值求解

中图分类号: O34 文献标志码: A 文章编号: 1005-2615(2024)02-0341-09

## Numerical Computation of Effective Stiffness of Gradient Plates Based on Asymptotic Homogenization

ZHANG Degang<sup>1</sup>, GU Chengzhang<sup>2</sup>, WEI Xiao<sup>2</sup>, QI Pengfei<sup>2</sup>, XU Liang<sup>1</sup>

(1. College of Aerospace Engineering, Nanjing University of Aeronautics & Astronautics, Nanjing 210016, China;

2. Structural System Research Laboratory, Aerospace System Engineering Shanghai, Shanghai 201109, China)

**Abstract:** Based on the asymptotic homogenization method of gradient plates, the unit cell problems and the effective stiffness of gradient plates are simplified, and the finite element solution is derived to achieve the efficient numerical solution of effective stiffness. Compared with the classical numerical homogenization method which can only deal with rectangular cells, this method can deal with general parallelogram microstructure and has good universality. The numerical examples verifies the correctness and feasibility of the numerical method proposed in this paper by comparing the deflection of the gradient stiffened plate and its corresponding equivalent homogeneous plate, and the relative error of the maximum deflection value is within 5%.

**Key words:** asymptotic homogenization; gradient stiffened plate; mapping function; effective stiffness; numerical solving

加筋结构是一种轻质<sup>[1]</sup>、高比强度/比刚度<sup>[2-3]</sup>、吸能能力<sup>[4-5]</sup>强、高阻尼<sup>[6]</sup>、热性能<sup>[7]</sup>良好和生物相容性<sup>[8]</sup>良好的结构, 具有宏观与微观两个尺度的结构特点, 这一结构特点使其在大幅降低材料使用率的同时能够保证结构的承载能力, 诸多优点使得加筋结构在航空航天<sup>[9-10]</sup>、汽车制造<sup>[11-12]</sup>及医

疗<sup>[13]</sup>等领域有着很大的应用前景与空间。

加筋板结构一般分为两类: 周期加筋板结构和梯度加筋板结构, 由于加筋结构跨尺度的特点, 采用渐近均匀化方法处理此类结构比较好。针对周期加筋结构已经有了比较充分的研究, 20 世纪 60 年代, 人们开始提出使用力学均匀化方法来模

**基金项目:** 国家自然科学基金青年基金(12002159); 江苏省自然科学基金青年基金(BK20200411); 大连理工大学工业装备结构分析国家重点实验室开放基金(GZ20101)。

**收稿日期:** 2023-08-02; **修订日期:** 2023-10-31

**通信作者:** 徐亮, 男, 讲师, E-mail: xuliang2018@nuaa.edu.cn。

**引用格式:** 张德纲, 顾铖璋, 韦 啸, 等. 基于渐近均匀化的梯度板等效刚度数值计算[J]. 南京航空航天大学学报, 2024, 56(2): 341-349. ZHANG Degang, GU Chengzhang, WEI Xiao, et al. Numerical computation of effective stiffness of gradient plates based on asymptotic homogenization[J]. Journal of Nanjing University of Aeronautics & Astronautics, 2024, 56(2): 341-349.

拟预测复合材料的等效力学性能,核心思想是使用均质材料来代替要研究的复合材料,使它们在力学场作用下有着相近的力学行为。基于多尺度的渐近分析<sup>[14-16]</sup>和体积平均<sup>[17-20]</sup>的均匀化方法已被一些研究人员用于研究周期加筋板。在基于等效应变能的均匀化方法中,通过非均匀材料中施加均匀应力或应变场的边界条件,使得非均匀材料中的应变能值与等效均匀材料中的应变能值相等,从而得到非均匀材料的力学等效性质<sup>[21]</sup>,在Hohe<sup>[17]</sup>的工作中,这种均匀化方法用于确定具有六边形蜂窝夹层板的等效刚度矩阵。在Alecci等<sup>[18]</sup>的工作中,开发了基于等效应变能的均匀化方法数值程序,用于评估嵌入形状记忆合金丝的周期加筋板力学行为。在Lebée等<sup>[19]</sup>的工作中,基于等效应变能的均匀化方法与弯曲梯度板理论<sup>[22]</sup>一起使用,获得了蜂窝夹层加筋板的等效剪切刚度张量。周期加筋结构相较于实体结构,重量大幅降低,物理性质、力学性能也更为优异<sup>[23]</sup>。但周期加筋结构相较于梯度加筋结构,设计自由度较低,仍属于未优化的均质分布结构<sup>[24-25]</sup>,这主要是因为周期加筋结构既没有考虑结构各部分承载不均的情况,也没有考虑结构最优的传力路径,未能进一步提升加筋结构的轻量化效率,使得加筋结构的潜能未能充分发挥<sup>[13]</sup>。

周期加筋板等效刚度的求解已经有了比较完善的发展,但目前梯度加筋板等效刚度的求解方法的发展还不够完善。常见的梯度加筋板根据其梯度变化方式一般可分为两类:第一类是矩形单胞内微结构的几何参数(体分比、转角、半径等)呈梯度变化,这类梯度加筋板由于其单胞是规则的矩形形状,仍然可以用周期加筋板等效刚度求解方法求解

其等效刚度;第二类是通过引入映射函数来实现梯度变化的板,这类板的单胞不再是规则的矩形结构,一般是平行四边形结构,无法用经典的周期加筋板等效刚度计算方法来求解其等效刚度。目前,Zhu等<sup>[26]</sup>已经实现了通过引入映射函数来实现梯度变化的非均质材料等效刚度求解,并在此基础上实现了梯度加筋材料的优化设计工作<sup>[27-30]</sup>。Xu等<sup>[31]</sup>将梯度加筋板映射为周期加筋板,在矩形单胞域内完成了梯度加筋板等效刚度的求解工作,该方法会导致雅可比矩阵出现在单胞方程求解的积分当中,就会导致求解时编程复杂困难,由于雅可比矩阵在刚度阵中出现,也无法将该方法集成到有限元软件当中。为有效实现梯度加筋板结构等效性质的有限元分析,本文将单胞方程及等效刚度求解转换到平行四边形单胞域内,推导其有限元求解列式及其在有限元软件中的数值实现流程,并将其应用到梯度板均匀化。

## 1 非均质梯度加筋板等效刚度

### 1.1 梯度加筋板的单胞方程及等效刚度列式

考虑如图1(a)中 $o\xi_1\xi_2\xi_3$ 坐标系下的梯度加筋板,由图1(b)周期加筋板经映射函数(式(1))映射而成。周期板矩形单胞定义在坐标系 $oy_1y_2y_3$ 中,如图1(d)所示,其中 $Y$ 为单胞域, $S'$ 为单胞非周期边界,矩形单胞的4个周期边界分别为 $\omega'_{1-}$ 、 $\omega'_{1+}$ 、 $\omega'_{2-}$ 、 $\omega'_{2+}$ ;梯度加筋板平行四边形单胞如图1(c)所示,所在坐标系为 $o\eta_1\eta_2\eta_3$ ,其中 $\eta$ 代表单胞的体域, $S$ 表示单胞非周期边界;梯度加筋板的单胞有4个周期边界,分别为 $\omega_{1-}$ 、 $\omega_{1+}$ 、 $\omega_{2-}$ 、 $\omega_{2+}$ ,映射转换前后,下标相同的周期边界一一对应。梯度加筋板单胞与周期

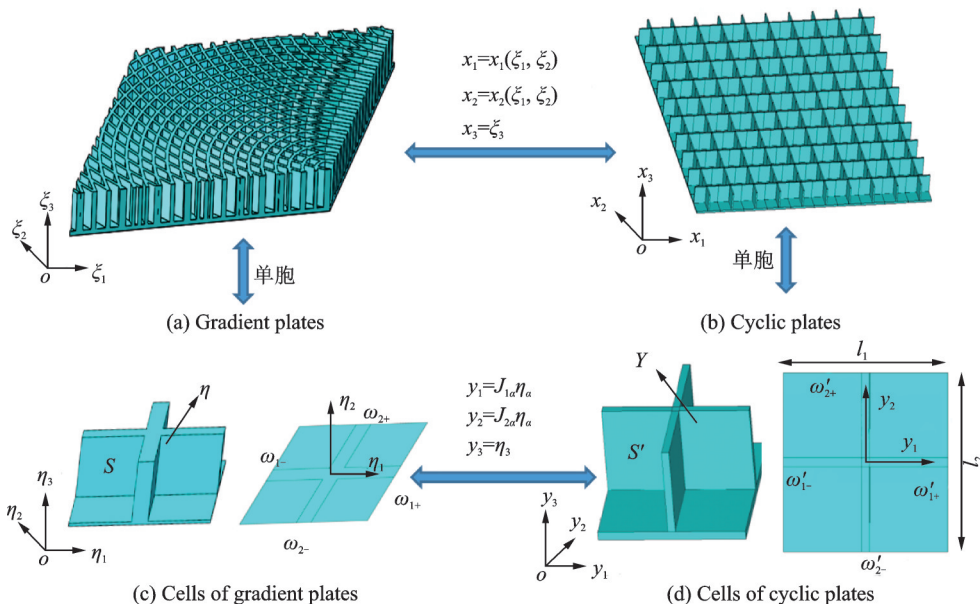


图1 梯度加筋板和周期加筋板及其单胞结构

Fig.1 Schematic diagram of gradient stiffened plates and periodic stiffened plates and their cell structures

加筋板单胞通过雅可比矩阵  $\mathbf{y} = \mathbf{J}\boldsymbol{\eta}$  相关联。

$$x_1 = x_1(\xi_1, \xi_2), x_2 = x_2(\xi_1, \xi_2), x_3 = \xi_3 \quad (1)$$

根据文献[31],梯度板等效刚度可通过求解定义在如图1(d)所示矩形单胞内的单胞方程计算得到。单胞方程定义为

$$\begin{cases} \mathbf{J}_{pj} \frac{\partial}{\partial y_p} \left( \mathbf{c}_{ija\beta} + \mathbf{c}_{ijkl} \mathbf{J}_{nl} \frac{\partial U_k^{a\beta}}{\partial y_n} \right) = 0 & \text{in } Y \\ \left( \mathbf{c}_{ija\beta} + \mathbf{c}_{ijkl} \mathbf{J}_{nl} \frac{\partial U_k^{a\beta}}{\partial y_n} \right) \mathbf{J}_{pj} \mathbf{n}_p = 0 & \text{on } S' \end{cases} \quad (2a)$$

$$\begin{cases} \mathbf{J}_{pj} \frac{\partial}{\partial y_p} \left( y_3 \mathbf{c}_{ija\beta} + \mathbf{c}_{ijkl} \mathbf{J}_{nl} \frac{\partial U_k^{*a\beta}}{\partial y_n} \right) = 0 & \text{in } Y \\ \left( y_3 \mathbf{c}_{ija\beta} + \mathbf{c}_{ijkl} \mathbf{J}_{nl} \frac{\partial U_k^{*a\beta}}{\partial y_n} \right) \mathbf{J}_{pj} \mathbf{n}_p = 0 & \text{on } S' \end{cases} \quad (2b)$$

式中:  $U_k^{a\beta}$  和  $U_k^{*a\beta}$  为广义位移,在单胞域  $Y$  内具有周期性;  $\mathbf{n}_p$  为外法线向量;  $\mathbf{c}$  为弹性张量。等效刚度计算为

$$\begin{cases} A_{\alpha\beta\gamma\mu} = \left\langle \left( \boldsymbol{\epsilon}_{ij}^{a\beta} + \mathbf{J}_{ij} \frac{\partial U_i^{a\beta}}{\partial y_j} \right) \mathbf{c}_{ijkl} \left( \boldsymbol{\epsilon}_{kl}^{\mu\nu} + \mathbf{J}_{pl} \frac{\partial U_k^{\mu\nu}}{\partial y_p} \right) \right\rangle \\ B_{\alpha\beta\gamma\mu} = \left\langle \left( \boldsymbol{\epsilon}_{ij}^{a\beta} + \mathbf{J}_{ij} \frac{\partial U_i^{a\beta}}{\partial y_j} \right) \mathbf{c}_{ijkl} \left( y_3 \boldsymbol{\epsilon}_{kl}^{\mu\nu} + \mathbf{J}_{pl} \frac{\partial U_k^{\mu\nu}}{\partial y_p} \right) \right\rangle \\ D_{\alpha\beta\gamma\mu} = \left\langle \left( y_3 \boldsymbol{\epsilon}_{ij}^{a\beta} + \mathbf{J}_{ij} \frac{\partial U_i^{*a\beta}}{\partial y_j} \right) \mathbf{c}_{ijkl} \left( y_3 \boldsymbol{\epsilon}_{kl}^{\mu\nu} + \mathbf{J}_{pl} \frac{\partial U_k^{\mu\nu}}{\partial y_p} \right) \right\rangle \end{cases} \quad (3)$$

其中

$$\boldsymbol{\epsilon}_{mn}^{a\beta} = \frac{1}{2} (\delta_{ma} \delta_{n\beta} + \delta_{m\beta} \delta_{na}), \langle \cdot \rangle = \frac{1}{|Y|} \int_Y \cdot \, dy \quad (4)$$

式中  $|Y|$  表示单胞在  $oY_1Y_2$  平面内的投影面积。

单胞方程式(2)显含雅可比矩阵系数,直接对其数值求解需要对包含雅可比矩阵的刚度阵及载荷向量进行数值积分,编程工作量很大。为方便其有限元求解,将式(2)转换至图1(c)中平行四边形单胞域  $o\eta_1\eta_2\eta_3$  内求解,表达式为

$$\begin{cases} \frac{\partial}{\partial \eta_p} \left( \mathbf{c}_{ija\beta} + \mathbf{c}_{ijkl} \frac{\partial U_k^{a\beta}}{\partial \eta_l} \right) = 0 & \text{in } \eta \\ \left( \mathbf{c}_{ija\beta} + \mathbf{c}_{ijkl} \frac{\partial U_k^{a\beta}}{\partial \eta_l} \right) \mathbf{n}_p = 0 & \text{on } S \end{cases} \quad (5a)$$

$$\begin{cases} \frac{\partial}{\partial \eta_p} \left( \eta_3 \mathbf{c}_{ija\beta} + \mathbf{c}_{ijkl} \frac{\partial U_k^{*a\beta}}{\partial \eta_l} \right) = 0 & \text{in } \eta \\ \left( \eta_3 \mathbf{c}_{ija\beta} + \mathbf{c}_{ijkl} \frac{\partial U_k^{*a\beta}}{\partial \eta_l} \right) \mathbf{n}_p = 0 & \text{on } S \end{cases} \quad (5b)$$

式(5)中不再显含雅可比系数  $\mathbf{J}_{ij}$ , 对应梯度加筋板的等效刚度为

$$\begin{cases} A_{\alpha\beta\mu\nu} = \left\langle \left( \boldsymbol{\epsilon}_{ij}^{a\beta} + \frac{\partial U_i^{a\beta}}{\partial \eta_q} \right) \mathbf{c}_{ijkl} \left( \boldsymbol{\epsilon}_{kl}^{\mu\nu} + \frac{\partial U_k^{\mu\nu}}{\partial \eta_p} \right) \right\rangle \\ B_{\alpha\beta\mu\nu} = \left\langle \left( \boldsymbol{\epsilon}_{ij}^{a\beta} + \frac{\partial U_i^{a\beta}}{\partial \eta_q} \right) \mathbf{c}_{ijkl} \left( \eta_3 \boldsymbol{\epsilon}_{kl}^{\mu\nu} + \frac{\partial U_k^{\mu\nu}}{\partial \eta_p} \right) \right\rangle \\ D_{\alpha\beta\mu\nu} = \left\langle \left( \eta_3 \boldsymbol{\epsilon}_{ij}^{a\beta} + \frac{\partial U_i^{*a\beta}}{\partial \eta_q} \right) \mathbf{c}_{ijkl} \left( \eta_3 \boldsymbol{\epsilon}_{kl}^{\mu\nu} + \frac{\partial U_k^{\mu\nu}}{\partial \eta_p} \right) \right\rangle \end{cases} \quad (6)$$

其中

$$\langle \cdot \rangle = \frac{1}{|\eta|} \int_{\eta} \cdot \, d\eta \quad (7)$$

进一步引入周期位移场  $\mathbf{V}^{\alpha\beta}$ ,  $\mathbf{V}^{*\alpha\beta}$  如下<sup>[32]</sup>

$$\begin{aligned} \mathbf{V}^{11} &= \begin{Bmatrix} \eta_1 \\ 0 \\ 0 \end{Bmatrix}, \mathbf{V}^{22} = \begin{Bmatrix} 0 \\ \eta_2 \\ 0 \end{Bmatrix}, \mathbf{V}^{12} = \begin{Bmatrix} \frac{\eta_2}{2} \\ \frac{\eta_1}{2} \\ 0 \end{Bmatrix}, \mathbf{V}^{*11} = \\ & \begin{Bmatrix} \eta_3 \eta_1 \\ 0 \\ -\frac{\eta_1^2}{2} \end{Bmatrix}, \mathbf{V}^{*22} = \begin{Bmatrix} 0 \\ \eta_3 \eta_2 \\ -\frac{\eta_2^2}{2} \end{Bmatrix}, \mathbf{V}^{*12} = \begin{Bmatrix} \frac{\eta_3 \eta_2}{2} \\ \frac{\eta_3 \eta_1}{2} \\ -\frac{\eta_1 \eta_2}{2} \end{Bmatrix} \end{aligned} \quad (8)$$

令  $\mathbf{W}^{\alpha\beta} = \mathbf{U}^{\alpha\beta} + \mathbf{V}^{\alpha\beta}$ ,  $\mathbf{W}^{*\alpha\beta} = \mathbf{U}^{*\alpha\beta} + \mathbf{V}^{*\alpha\beta}$ , 将式

(8)代入式(5),单胞方程可简化为

$$\begin{cases} \frac{\partial b_{ij}^{a\beta}}{\partial \eta_p} = 0 & \text{in } Y \\ b_{ij}^{a\beta} \eta_p = 0 & \text{on } S \\ \mathbf{W}_k^{a\beta} |_{\omega_{i,+}} - \mathbf{W}_k^{a\beta} |_{\omega_{i,-}} = \Delta \mathbf{W}_k^{a\beta} & \text{on } \omega_{i,\pm} \\ b_{ij}^{a\beta} \eta_p |_{\omega_{i,-}} + b_{ij}^{a\beta} \eta_p |_{\omega_{i,+}} = 0 & \text{on } \omega_{i,\pm} \end{cases} \quad (9a)$$

$$\begin{cases} \frac{\partial b_{ij}^{*a\beta}}{\partial \eta_p} = 0 & \text{in } Y \\ b_{ij}^{*a\beta} \eta_p = 0 & \text{on } S \\ \mathbf{W}_k^{*a\beta} |_{\omega_{i,+}} - \mathbf{W}_k^{*a\beta} |_{\omega_{i,-}} = \Delta \mathbf{W}_k^{*a\beta} & \text{on } \omega_{i,\pm} \\ b_{ij}^{*a\beta} \eta_p |_{\omega_{i,-}} + b_{ij}^{*a\beta} \eta_p |_{\omega_{i,+}} = 0 & \text{on } \omega_{i,\pm} \end{cases} \quad (9b)$$

其中

$$\begin{aligned} b_{ij}^{a\beta} &= \mathbf{c}_{ijkl} \frac{\partial \mathbf{W}_k^{a\beta}}{\partial \eta_l}, b_{ij}^{*a\beta} = \mathbf{c}_{ijkl} \frac{\partial \mathbf{W}_k^{*a\beta}}{\partial \eta_l}, \\ \Delta \mathbf{W}_k^{a\beta} |_{\omega_i} &= \mathbf{W}_k^{a\beta} |_{\omega_{i,+}} - \mathbf{W}_k^{a\beta} |_{\omega_{i,-}} = \mathbf{V}^{a\beta} |_{\omega_{i,+}} - \mathbf{V}^{a\beta} |_{\omega_{i,-}}, \\ \Delta \mathbf{W}_k^{*a\beta} |_{\omega_i} &= \mathbf{W}_k^{*a\beta} |_{\omega_{i,+}} - \mathbf{W}_k^{*a\beta} |_{\omega_{i,-}} = \mathbf{V}^{*a\beta} |_{\omega_{i,+}} - \mathbf{V}^{*a\beta} |_{\omega_{i,-}} \end{aligned} \quad (10)$$

得到沿  $\eta_1, \eta_2$  轴方向的平面拉伸以及在  $\eta_1\eta_2$  平面内剪切,板绕  $\eta_1, \eta_2$  轴弯曲变形以及板绕  $\eta_3$  轴扭转变形对应的差值边界条件分别为

$$\left\{ \begin{aligned}
 \Delta W^{11} \Big|_{\omega_i} &= \begin{Bmatrix} \eta_1 \\ 0 \\ 0 \end{Bmatrix}_{\omega_{i+}} - \begin{Bmatrix} \eta_1 \\ 0 \\ 0 \end{Bmatrix}_{\omega_{i-}} \\
 \Delta W^{22} \Big|_{\omega_i} &= \begin{Bmatrix} 0 \\ \eta_2 \\ 0 \end{Bmatrix}_{\omega_{i+}} - \begin{Bmatrix} 0 \\ \eta_2 \\ 0 \end{Bmatrix}_{\omega_{i-}} \\
 \Delta W^{12} \Big|_{\omega_i} &= \begin{Bmatrix} \frac{\eta_2}{2} \\ \eta_1 \\ 0 \end{Bmatrix}_{\omega_{i+}} - \begin{Bmatrix} \frac{\eta_2}{2} \\ \eta_1 \\ 0 \end{Bmatrix}_{\omega_{i-}} \\
 \Delta W^{*11} \Big|_{\omega_i} &= \begin{Bmatrix} \eta_3 \eta_1 \\ 0 \\ \frac{\eta_1^2}{2} \end{Bmatrix}_{\omega_{i+}} - \begin{Bmatrix} \eta_3 \eta_1 \\ 0 \\ \frac{\eta_1^2}{2} \end{Bmatrix}_{\omega_{i-}} \\
 \Delta W^{*22} \Big|_{\omega_i} &= \begin{Bmatrix} 0 \\ \eta_3 \eta_2 \\ \frac{\eta_2^2}{2} \end{Bmatrix}_{\omega_{i+}} - \begin{Bmatrix} 0 \\ \eta_3 \eta_2 \\ \frac{\eta_2^2}{2} \end{Bmatrix}_{\omega_{i-}} \\
 \Delta W^{*12} \Big|_{\omega_i} &= \begin{Bmatrix} \frac{\eta_3 \eta_2}{2} \\ \eta_3 \eta_1 \\ \frac{\eta_1 \eta_2}{2} \end{Bmatrix}_{\omega_{i+}} - \begin{Bmatrix} \frac{\eta_3 \eta_2}{2} \\ \eta_3 \eta_1 \\ \frac{\eta_1 \eta_2}{2} \end{Bmatrix}_{\omega_{i-}}
 \end{aligned} \right. \quad (11)$$

式中： $i$ 均取1和2,相同下标不求和。在平行四边形单胞域内进行有限元求解具有以下优势:(1)单胞方程不再显含雅可比矩阵;(2)仅需施加位移边界条件,无需进行载荷向量的组集。

### 1.2 梯度加筋板等效刚度有限元数值实现

前文已给出梯度加筋板的单胞方程及等效刚度理论求解列式,本节推导其有限元求解列式,并将其在有限元软件中实现。单胞方程(5)的等效积分弱形式为

$$\left\{ \begin{aligned}
 \int_{\eta} c_{ijkl} \frac{\partial \delta W_i^{\alpha\beta}}{\partial \eta_j} \frac{\partial W_k^{\alpha\beta}}{\partial \eta_l} d\eta &= 0 \\
 \int_{\eta} c_{ijkl} \frac{\partial \delta W_i^{*\alpha\beta}}{\partial \eta_j} \frac{\partial W_k^{*\alpha\beta}}{\partial \eta_l} d\eta &= 0
 \end{aligned} \right. \quad (12)$$

有限元离散后得

$$W^{\alpha\beta} k W^{\alpha\beta} = 0, W^{*\alpha\beta} k W^{*\alpha\beta} = 0 \quad (13)$$

式中： $k$ 为总刚度,  $k = \sum_{e=1}^{n_e} k_e$ ,  $k_e$ 为单元刚度,  $n_e$ 为离散后的单元总数,下标 $e$ 表示对应于第 $e$ 个单元的向量值,  $\alpha, \beta=1, 2$ 。由于位移  $W^{\alpha\beta}$ 、 $W^{*\alpha\beta}$ 满足周期边界条件式(11),并非独立自由度,设其独立自由度为主自由度,如图2中红框区域所示,以下标 $m$ 表示。图2中边界  $\omega'_{1-}$ 和  $\omega'_{2-}$ 为主自由度边界,根据两个主自由度边界的边界条件可推算出边界

$\omega'_{1+}$ 和  $\omega'_{2+}$ 对应的边界条件,主自由度和整体自由度的转换关系为<sup>[32]</sup>。

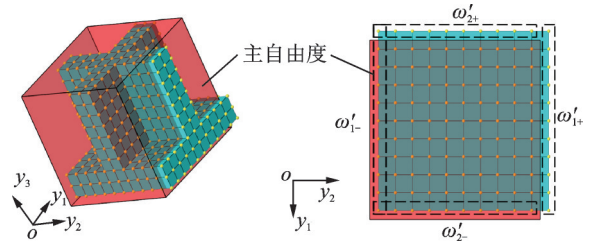


图2 主自由度区域

Fig.2 Master degrees of freedom region

$${}^n W^{\alpha\beta} = T^T {}^n W_m^{\alpha\beta} + \Delta {}^n W^{\alpha\beta}, {}^n W^{*\alpha\beta} = T^T {}^n W_m^{*\alpha\beta} + \Delta {}^n W^{*\alpha\beta} \quad (14)$$

式中  $T$  矩阵为主自由度和从自由度的转换矩阵<sup>[32]</sup>,由0和1组成。将式(14)代入式(13)得

$$T^T k T {}^n W_m^{\alpha\beta} = -T^T k \Delta {}^n W^{\alpha\beta}, T^T k T {}^n W_m^{*\alpha\beta} = -T^T k \Delta {}^n W^{*\alpha\beta} \quad (15)$$

根据式(14, 15),等效刚度的有限元求解列式为

$$A_{\alpha\beta\mu\nu} = \frac{1}{|\eta|} ({}^n W^{\alpha\beta})^T k {}^n W^{\mu\nu}, B_{\alpha\beta\mu\nu} = \frac{1}{|\eta|} ({}^n W^{\alpha\beta})^T k {}^n W^{*\mu\nu}, D_{\alpha\beta\mu\nu} = \frac{1}{|\eta|} ({}^n W^{*\alpha\beta})^T k {}^n W^{*\mu\nu} \quad (16)$$

式中： $\alpha, \beta, \mu, \nu=1, 2$ ;  $|\eta|$ 表示单胞在  $o\eta_1\eta_2\eta_3$  坐标系下的投影面积,满足

$$|\eta| = |Y| \cdot |J| \quad (17)$$

令  $F^{\alpha\beta} = k W^{\alpha\beta}$ ,  $F^{*\alpha\beta} = k W^{*\alpha\beta}$ ,其中  $F^{\alpha\beta}$ 、 $F^{*\alpha\beta}$ 为节点力。则式(16)可以改写为

$$A_{\alpha\beta\mu\nu} = \frac{1}{|\eta|} (W^{\alpha\beta})^T F^{\mu\nu}, B_{\alpha\beta\mu\nu} = \frac{1}{|\eta|} (W^{*\alpha\beta})^T F^{\mu\nu} = \frac{1}{|\eta|} (W^{\alpha\beta})^T F^{*\mu\nu}, D_{\alpha\beta\mu\nu} = \frac{1}{|\eta|} (W^{*\alpha\beta})^T F^{*\mu\nu} \quad (18)$$

下面给出等效刚度在有限元软件中的数值实现步骤:

**步骤1** 创建如图1(c)所示的单胞及其有限元模型,并进行网格划分;

**步骤2** 在有限元软件中通过添加耦合约束对周期边界根据式(11)施加模型位移边界条件,限制刚体位移,进行静力分析,提取节点位移  $W^{\alpha\beta}$ 、 $W^{*\alpha\beta}$  ( $\alpha, \beta=1, 2$ );

**步骤3** 将位移  $W^{\alpha\beta}$ 、 $W^{*\alpha\beta}$ 施加至单胞,数值分析得到节点力  $F^{\alpha\beta}$ 、 $F^{*\alpha\beta}$  ( $\alpha, \beta=1, 2$ );

**步骤4** 根据式(18)求解得到梯度加筋板的等效刚度。

## 2 数值算例

基于 1.2 节数值求解流程,采用 ANSYS 软件 APDL 编程实现等效刚度的计算。算例的单位均为无量纲参数;并通过板的挠度云图来验证等效刚度计算结果的正确性。

### 2.1 凹角蜂窝板等效刚度验证

算例 1 为如图 3 所示的凹角蜂窝板,其在  $o y_1 y_2 y_3$  坐标系下,  $l_{11}=17.32, l_{12}=60, h_{11}=10, h_{12}=1$ , 肋板厚度一致均为  $t_{11}=2$ ;雅可比矩阵系数分别

为  $J_{11}=0.578, J_{12}=-0.333, J_{22}=1.155, J_{33}=1$ ;映射变化后的尺寸可根据映射关系求出。

采用 solid186 单元进行模型网格划分,梯度加筋板单胞等效刚度的计算结果如表 1(结果已通过网格收敛性验证)所示。Wang 等<sup>[33-34]</sup>采用均匀化方法做过类似的工作,根据 Wang 等提出的方法对该算例进行等效刚度数值求解,经过网格收敛性验证之后得到结果。对比本文方法及 Wang 等的方法得出的结果可知,相对误差均在 5% 以内,验证了该方法的可行性。

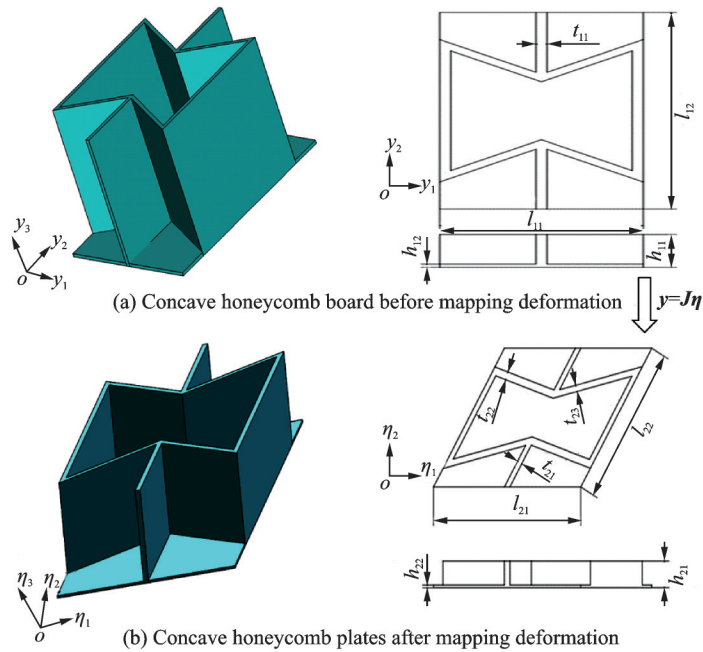


图 3 映射前后蜂窝板单胞模型

Fig.3 Cell model of honeycomb plates before and after mapping deformation

表 1 凹角蜂窝板模型等效刚度计算结果

Table 1 Calculation results of equivalent stiffness of concave honeycomb plate model

| 参数                        | $A_{1111}$ | $A_{1122}$ | $A_{1112}$ | $A_{2222}$ | $A_{2212}$ | $A_{1212}$ | $B_{1111}$ | $B_{1122}$ | $B_{1112}$ |
|---------------------------|------------|------------|------------|------------|------------|------------|------------|------------|------------|
| 本方法                       | 1.34       | $3.07e-1$  | $-1.43e-2$ | 1.17       | $3.09e-2$  | $4.14e-1$  | 1.08       | $-2.40e-1$ | $-1.34e-1$ |
| Wang 等 <sup>[33-34]</sup> | 1.35       | $3.11e-1$  | $-1.52e-2$ | 1.18       | $3.34e-2$  | $4.16e-1$  | 1.10       | $-2.64e-1$ | $-1.48e-1$ |
| 误差/%                      | 0.75       | 1.30       | 1.40       | 0.85       | 1.62       | 0.48       | 1.85       | 1.67       | 2.99       |
| 参数                        | $B_{2222}$ | $B_{2212}$ | $B_{1212}$ | $D_{1111}$ | $D_{1122}$ | $D_{1112}$ | $D_{2222}$ | $D_{2212}$ | $D_{1212}$ |
| 本方法                       | $1.06e-1$  | $5.41e-2$  | $3.78e-2$  | 7.03       | 1.50       | $8.32e-1$  | $7.60e-1$  | $3.36e-1$  | $2.75e-1$  |
| Wang 等 <sup>[33-34]</sup> | $1.03e-1$  | $5.93e-2$  | $3.73e-2$  | 7.12       | 1.59       | $9.07e-1$  | $7.91e-1$  | $3.65e-1$  | $2.87e-1$  |
| 误差/%                      | 2.91       | 0.37       | 1.34       | 1.28       | 1.33       | 3.00       | 4.08       | 2.68       | 4.36       |

为验证等效刚度的正确性,分别创建加筋板模型和均匀化后的均质板模型,两种板边界条件均为四边固支,在板的中心处施加大小为  $F=10^{-4}$  的集中力,仿真后得到的位移云图如图 4 所示。可以看出,两者位移云图吻合很好,图 4(a)中最大位移为 3.826,图 4(b)中最大位移为 3.866,相对误差为 1.04%。

### 2.2 Kagome 板等效刚度验证

算例 2 为如图 5(a)所示的 Kagome 加筋板单胞,尺寸参数为  $l_{31}=l_{32}=40, h_{31}=10, h_{32}=1$ , 肋板厚度一致均为  $t_{31}=1$ 。雅可比矩阵映射系数为  $J_{11}=0.500, J_{12}=-0.289, J_{22}=0.577, J_{33}=1$ ;通过坐标转化后得到梯度板平行四边形单胞,如图 5(b)所示。

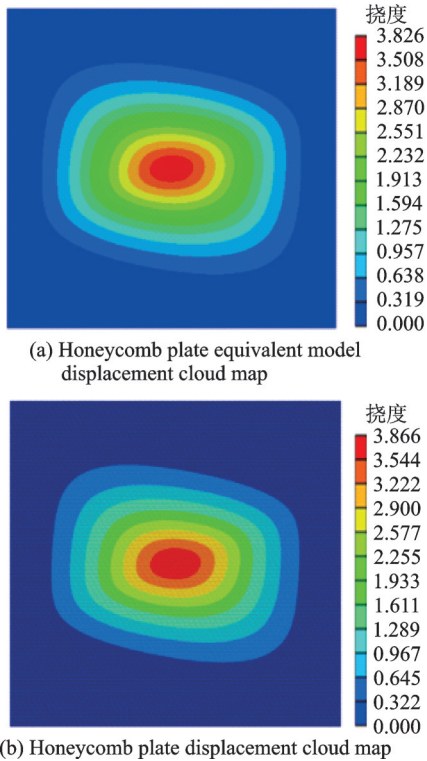


图4 凹角蜂窝板模型仿真验证结果

Fig.4 Simulation verification results of concave honeycomb plate model

经网格收敛性验证后的等效刚度系数如表2所示。同时根据 Wang 等提出的方法对该算例进行等效刚度数值求解,经过网格收敛性验证之后得到结果。对比本文方法及 Wang 等方法得出的结果可知,相对误差均在5%以内,验证了该方法的可行性。

类似地,对均匀板及加筋板施加四边固支边界条件,在板的中心处施加大小为  $F=10^{-4}$  的集中力,仿真后得到的位移云图如图6所示。可以看出,两个云图同样吻合,图6(a)中最大位移为0.6856,图6(b)中最大位移为0.6581,相对误差为4.01%。

2.3 凹角蜂窝梯度板整体等效刚度验证

为验证本文方法可适用于梯度板结构,考虑采用如图7(a)所示的凹角蜂窝按照式(19)映射函数<sup>[31]</sup>构造的梯度板如图7(b)所示。

$$\begin{cases} y_1 = -\sqrt{\bar{\xi}_1^2 + \bar{\xi}_2^2} \arctan\left(\frac{\eta_1 - \bar{\xi}_1}{\eta_2 - \bar{\xi}_2}\right) \\ y_2 = \sqrt{\bar{\xi}_1^2 + \bar{\xi}_2^2} \arctan\left(\frac{\eta_1 - \bar{\xi}_1}{\bar{\xi}_2 - \eta_2}\right) \end{cases} \quad (19)$$

式中:  $\bar{\xi}_1 = \bar{\xi}_2 = -700, \bar{\xi}_1 = -800, \bar{\xi}_2 = 700$ , 梯度板单胞尺寸同图7(a),  $l_{s1} = 34.64, l_{s2} = 60, h_s = 9.5$ , 映射后梯度加筋板尺寸为  $1\ 200 \times 1\ 200 \times 9.5$ 。

均匀化后的板采用 Kirchhoff 矩形板单元进行网格划分,单元等效性质根据2.2节方法求解,有限元分析后位移云图如图8(a)所示。梯度加筋板采用 shell181 壳单元进行网格划分,四边固支,并在中点处施加大小为  $F=10^{-4}$  的集中载荷,有限元分析后挠度位移云图如图8(b)所示。可以看出,均匀化板与梯度加筋板的位移云图一致,均匀化板最大挠度为0.4310,梯度板最大挠度为0.4268,两者相差0.98%,验证了等效刚度的正确性。

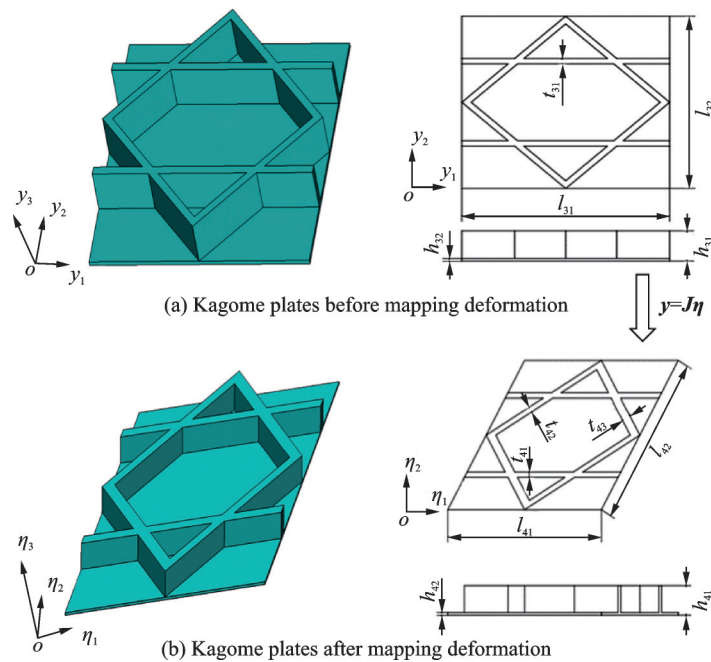
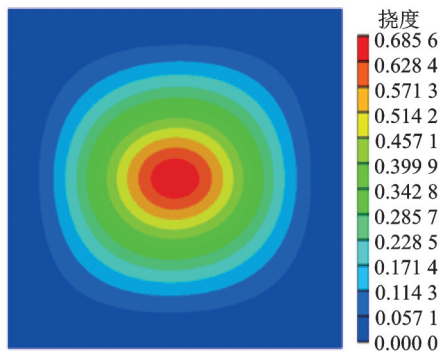


图5 映射前后 Kagome 板模型

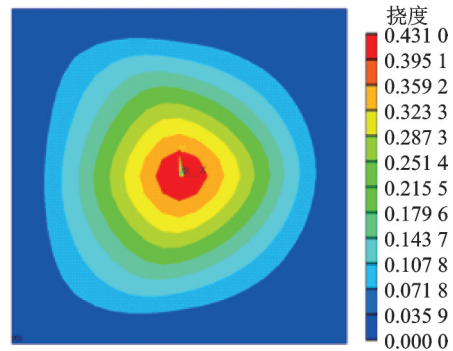
Fig.5 Kagome plate model before and after mapping deformation

表 2 Kagome 板模型等效刚度计算结果  
Table 2 Equivalent stiffness calculation results of Kagome plates

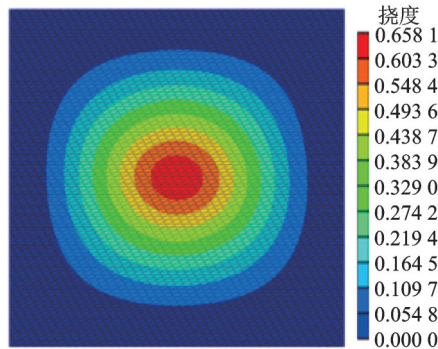
| 参数                        | $A_{1111}$ | $A_{1122}$ | $A_{1112}$ | $A_{2222}$ | $A_{2212}$ | $A_{1212}$ | $B_{1111}$ | $B_{1122}$ | $B_{1112}$ |
|---------------------------|------------|------------|------------|------------|------------|------------|------------|------------|------------|
| 本方法                       | 1.71       | 4.28e-1    | 5.49e-2    | 1.25       | -2.37e-2   | 4.70e-1    | 3.00e-1    | 4.86e-1    | 2.79e-1    |
| Wang 等 <sup>[33-34]</sup> | 1.79       | 4.35e-1    | 5.30e-2    | 1.28       | -2.47e-2   | 4.86e-1    | 2.94e-1    | 4.71e-1    | 2.91e-1    |
| 误差/%                      | 4.68       | 1.64       | 3.58       | 2.40       | -4.05      | 3.40       | 2.04       | 3.18       | 4.30       |
| 参数                        | $B_{2222}$ | $B_{2212}$ | $B_{1212}$ | $D_{1111}$ | $D_{1122}$ | $D_{1112}$ | $D_{2222}$ | $D_{2212}$ | $D_{1212}$ |
| 本方法                       | 6.40e-1    | -9.71e-2   | 3.64e-1    | 19.2       | 3.09       | 1.75       | 4.16       | -6.10e-1   | 2.36       |
| Wang 等 <sup>[33-34]</sup> | 6.52e-1    | -9.97e-2   | 3.56e-1    | 18.7       | 3.19       | 1.83       | 4.34       | -6.21e-1   | 2.46       |
| 误差/%                      | 1.88       | 2.61       | 2.25       | 2.67       | 3.24       | 4.57       | 4.33       | 1.80       | 4.24       |



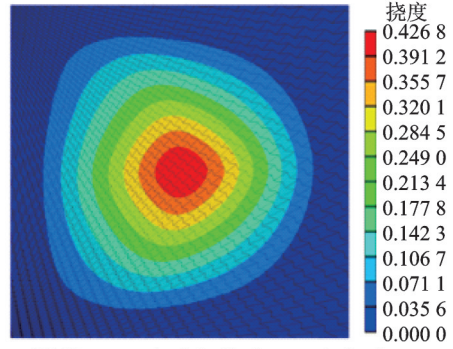
(a) Equivalent displacement cloud plot of the Kagome plates



(a) Equivalent displacement cloud plot of honeycomb plates



(b) Displacement cloud plot of the Kagome plates



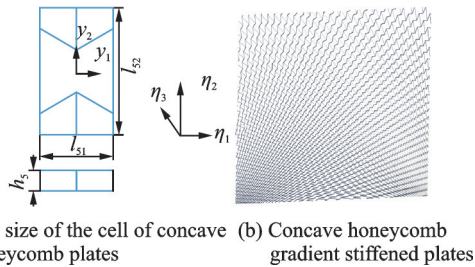
(b) Honeycomb plate displacement cloud plot calculated by OptiStruct

图 6 Kagome 板模型仿真验证结果

Fig.6 Simulation verification results of Kagome plates

图 8 两种方法获得的凹角蜂窝梯度加筋板位移云图

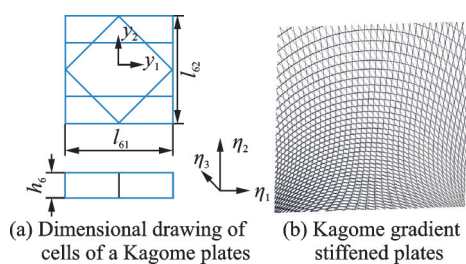
Fig.8 Displacement cloud plot of concave honeycomb gradient stiffened plates calculated by two methods



(a) The size of the cell of concave honeycomb plates (b) Concave honeycomb gradient stiffened plates

图 7 凹角蜂窝板单胞及整体模型

Fig.7 Single cell and integral model of concave honeycomb plates



(a) Dimensional drawing of cells of a Kagome plates (b) Kagome gradient stiffened plates

图 9 Kagome 梯度加筋板单胞及整体模型

Fig.9 Cell and overall model of Kagome gradient stiffened plates

2.4 Kagome 梯度板整体等效刚度验证

为验证本文方法可适用于梯度板结构,考虑采用如图 9(a)所示的凹角蜂窝按式(20)映射函数<sup>[31]</sup>构造的梯度板,如图 9(b)所示。

$$\begin{cases} y_1 = -\sqrt{\bar{\xi}_1^2 + \bar{\xi}_2^2} \arctan\left(\frac{\eta_2 - \bar{\xi}_2}{\eta_1 - \bar{\xi}_1}\right) \\ y_2 = \sqrt{\bar{\xi}_1^2 + \bar{\xi}_2^2} \arctan\left(\frac{\eta_2 - \bar{\xi}_2}{\bar{\xi}_1 - \eta_1}\right) \end{cases} \quad (20)$$

式中： $\bar{\xi}_1 = \bar{\xi}_2 = -600$ ,  $\bar{\xi}_1 = 700$ ,  $\bar{\xi}_2 = -600$ ,  $l_{61} = 34.64$ ,  $l_{62} = 60$ ,  $h_6 = 9.5$ , 映射后梯度加筋板尺寸为  $960 \times 960 \times 9.5$ 。

均匀化后的板采用 Kirchhoff 矩形板单元进行网格划分, 单元等效性质根据 2.2 节方法求解, 有限元分析后位移云图如图 10(a) 所示。梯度加筋板采用 shell181 壳单元进行网格划分, 四边固支, 并在中点处施加大小为  $F = 10^{-4}$  的集中载荷, 有限元分析后挠度位移云图如图 10(b) 所示。可以看出, 均匀化板与梯度加筋板的位移云图一致, 均匀化板最大挠度为 0.062 1, 梯度板最大挠度为 0.064 1, 两者相差 3.22%, 验证了等效刚度的正确性。

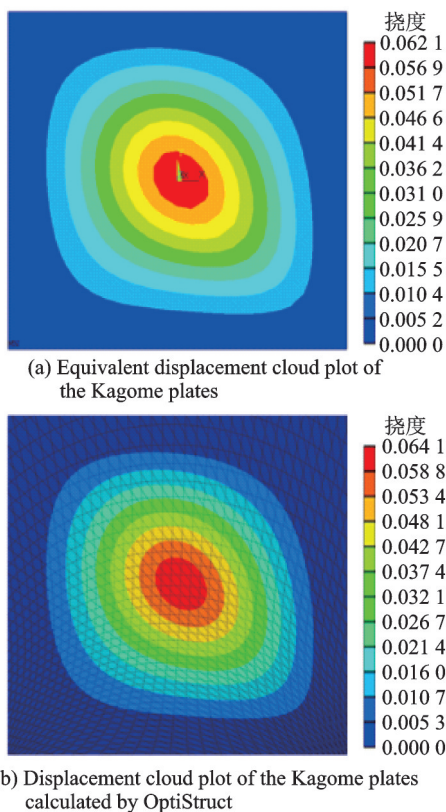


图 10 两种方法获得的 Kagome 梯度加筋板位移云图

Fig.10 Displacement cloud plot of the Kagome gradient stiffened plates obtained by two methods

### 3 结 论

基于梯度加筋板结构的渐近均匀化方法, 通过映射函数的雅可比矩阵, 将其单胞方程由矩形单胞域转换为平行四边形单胞域, 避免了雅可比系数显式出现在单胞方程中, 从而简化了单胞方程的求解。在此基础上推导了单胞方程的有限元列式及其在有限元软件中的求解流程, 实现了一般平行四边形单胞等效刚度的有限元数值求解。

分别对凹蜂窝梯度加筋板以及 Kagome 梯度加筋板进行数值分析, 并通过对比均匀化板和梯度

加筋板的位移云图验证了本文方法的正确性。

### 参考文献:

- [1] MACONACHIE T, LEARY M, LOZANOVSKI B, et al. SLM lattice structures: Properties, performance, applications and challenges[J]. *Materials & Design*, 2019, 183: 108-137.
- [2] LI D W, LIAO W H, DAI N, et al. Anisotropic design and optimization of conformal gradient lattice structures[J]. *Computer-Aided Design*, 2020, 119(3): 102787.
- [3] ZHU Y C, LI S S, GUO X, et al. A novel asymptotic-analysis-based homogenisation approach towards fast design of infill graded microstructures[J]. *Mechanics and Physics of Solids*, 2019, 124: 612-633.
- [4] TAMBURRINO F, GRAZIOSI S, BORDEGONI M. The design process of additively manufactured mesoscale lattice structures: A review[J]. *Computing and Information Science in Engineering*, 2018, 18(4): 040801.
- [5] SAEDI D S, MASOOD S H, FAIZAN U R M, et al. Mechanical properties and energy absorption capability of functionally graded F2BCC lattice fabricated by SLM[J]. *Materials & Design*, 2018, 144: 32-44.
- [6] CHEN Y, ZHAO B H, LIU X N, et al. Highly anisotropic hexagonal lattice material for low frequency water sound insulation[J]. *Extreme Mechanics Letters*, 2020, 40: 100916.
- [7] SMITH S, SELO R R J, DAVIS A W, et al. Thermal conductivity of TPMS lattice structures manufactured via laser powder bed fusion[J]. *Additive Manufacturing*, 2019, 30: 100846.
- [8] ZHANG L C, CHEN L Y. A review on biomedical titanium alloys: Recent progress and prospect[J]. *Advanced Engineering Materials*, 2019, 21(4): 1801215.
- [9] 周松. 基于 SLM 的金属 3D 打印轻量化技术及其应用研究[D]. 杭州: 浙江大学, 2017.
- [10] ZHOU Song. The study and application on lightweight 3D metal printing based on selective laser melting technology[D]. Hangzhou: Zhejiang University, 2017.
- [11] JIN X, LI G X, LI U E, et al. Lightweight design for servo frame based on lattice material [C]//Proceedings of the 4th International Conference on Advanced Composite Materials and Manufacturing Engineering (ACMME). [S.l.]: IOP, 2017: 012035.
- [12] YIN S, CHEN H Y, WU Y B, et al. Introducing composite lattice core sandwich structure as an alternative proposal for engine hood[J]. *Composite Structure*, 2018, 201: 131-140.
- [12] 廖中源, 王英俊, 王书亭. 基于拓扑优化的变密度加



- 筋结构体优化设计方法[J]. 机械工程学报, 2019, 55(8): 65-72.
- LIAO Zhongyuan, WANG Yingjun, WANG Shuting. Graded-density lattice structure optimization design based on topology optimization[J]. Journal of Mechanical Engineering, 2019, 55(8): 65-72.
- [13] DU P A, YADROITSAVA I, YADROITSEV I, et al. Numerical comparison of lattice unit cell designs for medical implants by additive manufacturing[J]. Virtual and Physical Prototyping, 2018, 13(4): 266-281.
- [14] CAILLERIE D, NEDELEC J. Thin elastic and periodic plates[J]. Mathematical. Methods in the Applied Sciences, 1984, 6(1): 159-191.
- [15] KOHN R V, VOGELIUS M. A new model for thin plates with rapidly varying thickness[J]. Solids Structures, 1984, 20: 333-350.
- [16] CECCHI A, SAB K. Out of plane model for heterogeneous periodic materials: The case of masonry[J]. A Solids, 2002, 21: 715-746.
- [17] HOHE J. A direct homogenisation approach for determination of the stiffness matrix for microheterogeneous plates with application to sandwich panels[J]. Composites B Engineering, 2003, 34: 615-626.
- [18] ALECCI V, BATI S B, RANOCCHIAI G. Numerical homogenization techniques for the evaluation of mechanical behavior of a composite with SMA inclusions [J]. Mechanic & Structure, 2009, 4: 1675-1688.
- [19] LEBÉE A, SAB K. Homogenization of cellular sandwich panels[J]. Comptes Rendus Mécanique, 2012, 340: 320-337.
- [20] LEBÉE A, SAB K. Homogenization of a space frame as a thick plate: Application of the bending-gradient theory to a beam lattice[J]. Computers Structures, 2013, 127: 88-101.
- [21] HILL R. Elastic properties of reinforced solids: Some theoretical principles[J]. Mechanics Physics Solids, 1963, 11: 357-372.
- [22] LEBÉE A, SAB K. A bending-gradient model for thick plates [J]. Solids Structures, 2011, 48: 2878-2888.
- [23] 欧阳佳琛. 基于改进变密度法的功能梯度材料拓扑优化设计[D]. 武汉: 华中科技大学, 2016.
- OUYANG Jiachen. Topology optimization design of functionally graded materials based on modified variable density method[D]. Wuhan: Huazhong University of Science and Technology, 2016.
- [24] PANESAR A, ABDI M, HICKMAN D, et al. Strategies for functionally graded lattice structures derived using topology optimisation for additive manufacturing [J]. Additive Manufacturing, 2018, 19: 81-94.
- [25] 金鑫. 面向激光增材制造的变密度多胞结构优化设计与建模研究[D]. 长沙: 国防科技大学, 2018.
- JIN Xin. Optimal design and modeling of variable-density cellular structures for laser additive manufacturing [D]. Changsha: National University of Defense Technology, 2018.
- [26] ZHU Y, LI S, DU Z, et al. A novel asymptotic-analysis-based homogenisation approach towards fast design of infill graded microstructures[J]. Mechanics and Physics of Solids, 2019, 124: 612-633.
- [27] MA C, XUE D, LI S, et al. Compliance minimisation of smoothly varying multiscale structures using asymptotic analysis and machine learning[J]. Computer Methods in Applied Mechanics and Engineering, 2022, 395: 114861.
- [28] XUE D, ZHU Y, LI S, et al. On speeding up an asymptotic-analysis-based homogenisation scheme for designing gradient porous structured materials using a zoning strategy[J]. Structural and Multidisciplinary Optimization, 2020, 62: 457-473.
- [29] LIU C, DU Z, ZHU Y, et al. Optimal design of shell-graded-infill structures by a hybrid MMC-MMV approach[J]. Computer Methods in Applied Mechanics and Engineering, 2020, 369: 113187.
- [30] LI S, ZHU Y, GUO X. Optimisation of spatially varying orthotropic porous structures based on conformal mapping[J]. Computer Methods in Applied Mechanics and Engineering, 2022, 391: 114589.
- [31] XU L, ZHANG D G, ZHANG Y C, et al. Effective property calculation and its numerical implementation of spatially graded plate structures based on asymptotic homogenization[J]. Composite Structures, 2022, 300: 116165.
- [32] CAI Y W, XU L, CHENG G D. Novel numerical implementation of asymptotic homogenization method for periodic plate structures[J]. Solids Structures, 2014, 51(1): 284-92.
- [33] WANG D, ABDALL M M. Global and local buckling analysis of grid-stiffened composite panels [J]. Composite, 2015, 119: 767-776.
- [34] WANG D, ABDALL M M, et al. Sensitivity analysis for optimization design of non-uniform curved grid-stiffened composite (NCGC) structures[J]. Composite Structures, 2018, 193: 224-236.